Металлофиз. новейшие технол. / Metallofiz. Noveishie Tekhnol.
2018, т. 40, № 12, сс. 1675–1687/ DOI: 10.15407/mfint.40.12.1675
Оттиски доступны непосредственно от издателя
Фотокопирование разрешено только
в соответствии с лицензией

СТРОЕНИЕ И СВОЙСТВА НАНОРАЗМЕРНЫХ И МЕЗОСКОПИЧЕСКИХ МАТЕРИАЛОВ

PACS numbers: 02.70.Ns, 07.05.Tp, 36.40.-c, 61.46.Bc, 61.72.sh, 81.05.Zx, 81.07.Oj

The Estimation of Stability and Growth of F.C.C. Iron Nanocluster Containing the Impurity Atoms

N. V. Bondarenko and A. V. Nedolya

Zaporizhzhya National University,
66 Zhukovsky Str.,
69600 Zaporizhzhya, Ukraine

The energy of the isolated iron nanocluster is calculated by molecular mechanics method using Lennard-Jones potential depending on the position of impurities, *i.e.*, interstitial carbon atom and substitutional nickel atom. The cluster included a carbon atom drifted to the surface from an inner octahedral interstice along the $\langle 011 \rangle$ direction or through the tetrahedral interstice firstly in the $\langle 1\bar{1}1 \rangle$ direction and then in the $\langle 111 \rangle$ direction. One of the 14 iron atoms is replaced with a nickel atom in the position, which is changed during simulation. As determined, the positions of a nickel atom significantly affect the energy of the nanocluster. The calculation results in the case of f.c.c. nanocluster indicate that position of a carbon atom at the octahedral interstice is more energy-favourable than its position at the tetrahedral interstice. On the other hand, the potential barrier is smaller in the $\langle 1\bar{1}1 \rangle$ direction than in the $\langle 011 \rangle$ direction. This indicates that two ways for carbon atom drifting to the nanocluster surface are available. The changing of the nickel-atom position significantly influences on the height of the potential barriers of the octahedral and tetrahedral interstitial sites that gives a possibility to manipulate a carbon atom within the near-surface layer of nanocluster. Besides, a carbon atom affects the nanocluster-growth direction, which is estimated by the joining energy for the additional iron atom. The obtained results can be useful in medicine, biology and technologies of nanoelectromechanical systems (NEMS) where both nanoclusters and nanoparticles are used.

Key words: iron nanocluster, energy of nanocluster, impurity atoms, molecular mechanics method.

Corresponding author: Anatoliy Vasylyovych Nedolya
E-mail: avnedolya@hotmail.com

Citation: N. V. Bondarenko and A. V. Nedolya, The Estimation of Stability and Growth of F.C.C. Iron Nanocluster Containing the Impurity Atoms, *Metallofiz. Noveishie Tekhnol.*, **40**, No. 12: 1675–1687 (2018), DOI: 10.15407/mfint.40.12.1675.

Методою молекулярної механіки з використанням потенціялу Леннард-Джонса розраховано енергію ізольованого нанокластера заліза в залежності від положення атома Карбону як атома втілення та атома Ніклю як атома заміщення. Втілений у нанокластер атом Карбону дрейфував до поверхні із внутрішньої октапори або безпосередньо в напрямку $\langle 011 \rangle$, або через тетрапору спочатку в напрямку $\langle 1\bar{1}1 \rangle$, а потім у напрямку $\langle 111 \rangle$. Один з 14 атомів Феруму був заміщений атомом Ніклю, положення якого змінювалося під час моделювання. Було визначено, що положення атома Ніклю істотно впливає на енергію нанокластера. Результати розрахунків показали, що у випадку ГЦК-нанокластера положення атома Карбону в октапорі було більш енергетично вигідним, ніж у тетрапорі. З іншого боку, потенціяльний бар'єр у напрямку $\langle 1\bar{1}1 \rangle$ був менший, ніж у напрямку $\langle 011 \rangle$. Це вказує на існування двох способів дрейфу атома Карбону до поверхні нанокластера. Зміна положення атома Ніклю істотно впливала на висоту потенціяльних бар'єрів октаедричних і тетраедричних міжвузлів, що уможливлює маніпулювати атомом Карбону в приповерхневому шарі нанокластера. Крім цього, атом Карбону впливав на напрямок зростання нанокластера, який оцінювався за допомогою енергії приєднання додаткового атома Феруму. Дослідження може бути корисним у медицині, біології та технологіях наноелектромеханічних систем, де використовуються такі нанокластери та наночастинки.

Ключові слова: нанокластер заліза, енергія нанокластера, домішкові атоми, метод молекулярної механіки.

Методом молекулярной механики с использованием потенциала Леннард-Джонса рассчитана энергия изолированного нанокластера железа в зависимости от положения внедрённого атома углерода и замещённого атома никеля. Внедрённый в нанокластер атом углерода дрейфовал к поверхности из внутренней октапоры или непосредственно в направлении $\langle 011 \rangle$, или через тетрапору сначала в направлении $\langle 1\bar{1}1 \rangle$, а затем в направлении $\langle 111 \rangle$. Один из 14 атомов железа был замещён атомом никеля, положение которого менялось во время моделирования. Было определено, что положение атома никеля существенно влияет на энергию нанокластера. Результаты расчётов показали, что в случае ГЦК-нанокластера положение атома углерода в октапоре было более выгодным энергетически, чем в тетрапоре. С другой стороны, потенциальный барьер в направлении $\langle 1\bar{1}1 \rangle$ был меньше, чем в направлении $\langle 011 \rangle$. Это указывает на существование двух способов дрейфа атома углерода к поверхности нанокластера. Изменение положения атома никеля существенно влияло на высоту потенциальных барьеров октаэдрических и тетраэдрических междоузлий, что позволяет манипулировать атомом углерода в приповерхностном слое нанокластера. Кроме того, атом углерода влиял на направление роста нанокластера, что оценивалось с помощью энергии присоединения дополнительного атома железа. Исследование может быть полезным в медицине, биологии и технологиях наноэлектромеханических систем, в которых используются такие нанокластеры и наночастицы.

Ключевые слова: нанокластер железа, энергия нанокластера, примесные атомы, метод молекулярной механики.

(Received January 12, 2018)

1. INTRODUCTION

Usually, the nanostructured materials, nanoparticles, and nanoclusters are formed from traditional metal alloys under the influence of the extreme conditions: extrusion, multiple phase transitions, laser surface treatment, metal particles deposition from the vapour phase, *etc.*, [1, 2]. Also, the nanoclusters can be formed due to concentration changes in the local volume because of the presence of impurity atoms [3, 4]. Such local changes bounded the thermal vibrations of atoms in the surroundings where the nanoclusters formed during the non-equilibrium and high-speed processes [5–8]. In addition, the metastable nanophases can be formed because of the high cooling rate, the high degrees of deformation or both [9, 10].

The presence of impurities can affect both the melting processes and the catalytic properties of nanoparticles [11, 12] as well as the phase transitions [13] and peculiarities of atom interaction [14]. Either of it affects the nanoclusters growth, their stability, and shape [15–20].

The study of the metastable nanostructures and nanoclusters can help solve the problem of their stabilization, using the atoms of other types and control the self-organization process of the nanosystems.

2. MODEL

For the study, we chose an f.c.c. Fe–Ni–C nanocluster containing 15 atoms. All the f.c.c. cluster atoms are located on the surface or formed the surface, which simplified interpretation of calculation results. We assumed that such cluster is formed randomly at an initial time and contains one carbon atom and a nickel atom substituting iron atom. The system was considered as quasi-stable during the mean time between consecutive jumps of a nickel atom along the surface. Therefore, we took into account the statics only, when energy changes were evaluated using the method of molecular mechanics (MM+). We regarded such nanocluster as the nanosize analogy of the microscopic metastable γ-phase of the Fe–Ni–C alloy that was able to form under the influence of the non-equilibrium conditions and has been studied well before [21–25]. We performed the evaluation of energy empirically using the solution of the Newton equations' set:

$$m_i(d^2\mathbf{r}_i(t)/dt^2) = -\partial U(\mathbf{r}_{ij})/\partial\mathbf{r}_i + \mathbf{F}_i^{ex}, \quad (1)$$

where $\mathbf{F}_i^{ex}$ —the force that determines external interactions; $\mathbf{r}_i$ and $\mathbf{r}_j$— the coordinates of the interacting atoms; $\mathbf{r}_{ij} = \mathbf{r}_i - \mathbf{r}_j$;

$$U(r_{ij}) = 4\varepsilon_{kl}\sum_{i<j}[(\sigma_{kl}/r_{ij})^{12} - (\sigma_{kl}/r_{ij})^{6}], \quad (2)$$

where $\varepsilon_{kl} = (\varepsilon_{kk}\varepsilon_{ll})^{1/2}$—the bond energy and $\sigma_{kl} = (\sigma_{kk}+\sigma_{ll})/2$—the measure of the atomic size. The ε_{kl} and σ_{kl} were calculated using Lorenz–Berthelot mixing rule for atoms of k-th and l-th classes [26–31].

The choice of Lennard-Jones (LJ) potential was associating with the fact that the size of nanocluster was less than a critical size (less than 1 nm) and the random forming of f.c.c.-similar structure did not mean that it was crystalline in every sense of the word, because it was less than three coordination spheres.

Thus, for simplicity of calculations for the nanocluster, we preferred the generalized Lennard-Jones potential to other potentials (Buckingham potential or truncated LJ potential). The cluster surroundings were regarded as isotropic.

We calculated the energy difference between the carbon-atom position inside the octahedral or tetrahedral interstice in the nanocluster and current position during its drift to the surface [32]:

$$\Delta u = u(L) - u(0), \quad (3)$$

where L is a length of the carbon-atom path, $u = U(N)/N$—specific potential energy (in meV per atom), $U(N)$—the base cluster energy, N—atoms' quantity. The carbon-atom position in the central (internal) octahedral interstitial site (COIS) of a cluster was chosen as null (0) of the path length (L), conforming to the central symmetry of the nanocluster.

At first, the molecular dynamic (MD) and Langevin dynamic (LD) methods used for calculations also at 300 K. Deviations of the values Δu of specific energy changes in the vacuum did not exceed 1.5% (Fig. 1, *a*). The specific energy changes of the nanocluster in the hydrated coat by MM+, MD, LD as well as the Monte Carlo (MS) methods were calculated in addition (Fig. 1, *b*). Deviations between the values Δu of the difference in specific energy calculated by different methods did not exceed 3%. The difference between the specific energy changes in the case when the carbon atom was on the nanocluster surface in the vacuum as well in the hydrated coat shell consisted of about 5%.

Therefore, all calculations were carried out in vacuum using the MM+ method for such nanoscale taking into account the specific energies' changes. We simulated the carbon-atom drift to the nanocluster surface because of the influence of surface. Every possible position of nickel atom, which might replace the iron atom, was examining as an analogue of random diffused jumps of nickel atom. In such system, any energy changes may be possible under changing positions of the impurity atoms only. The 3.6 Å distance between the atoms was selected, which meet to the maximum of a potential barrier for more stability of f.c.c. nanocluster [33].

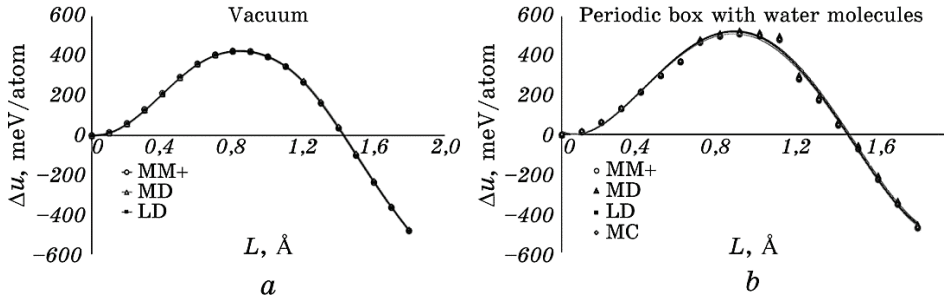

Fig. 1. The specific energy changes of the nanocluster in a vacuum (*a*) and in the hydrated coat (*b*), where: MM+—the molecular mechanic, MD—molecular dynamic, LD—Langevin dynamic, MC—Monte Carlo methods.

The cluster energy after the addition of an iron atom at a distance equal to 3.6 Å have compared in all configurations too:

$$u_{\pm i} = [U_{\pm i}(N+1) - U(N)]/N, \tag{4}$$

where $\Delta u_{\pm i}$—cluster specific energy, when an iron atom joins the *i*-side (meV/atom); *i*—*X*, *Y* or *Z*-axis, $U_{\pm i}(N+1)$—the growing cluster energy.

We also took into account the atom thermal vibrations energy ($\Delta\varepsilon_{kT}$) that was about 40 meV at the room temperature and it has been comparing to the growing cluster energy.

3. RESULTS AND DISCUSSION

3.1. The Estimation of the Direction of the Carbon-Atom Drift to the Surface

We defined two directions of a carbon-atom drift to the surface: the ⟨011⟩ direction (dark grey arrow) and the way $\langle\bar{1}11\rangle$ plus ⟨111⟩ (light grey arrows) for calculation (see a triangle on Fig. 2). The $\langle\bar{1}11\rangle$ plus ⟨111⟩ way passed through the tetrahedral interstitial site (TIS). Both directions were energy-favourable for the carbon atom because the cluster energy was almost twice smaller when the carbon atom was on the surface ($L = 1.8$) compared to its position in the central octahedral interstice ($L = 0$), due to the influence of the surface.

However, in the case when the carbon atom drifted towards the ⟨011⟩ direction, the potential barrier Δu (Δ) was higher than two potential barriers Δu_1 (Δ_1), Δu_2 (Δ_2) in the $\langle\bar{1}11\rangle$ plus ⟨111⟩ way (Fig. 3).

We compared the similar energies of the nanocluster at changing of nickel-atom position and determined its effect on the TIS potential barriers height. The potential barrier was lowest for the carbon atom that drifting using the ⟨011⟩ direction to the surface in the cases when

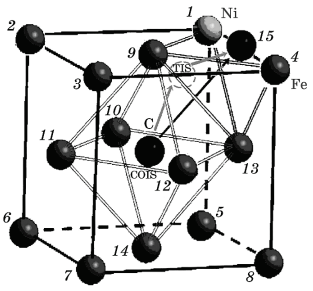

Fig. 2. The scheme of carbon-atom drift to the surface: dark grey arrow—in the ⟨011⟩ direction; light grey arrows—in the $\langle\bar{1}11\rangle$ plus ⟨111⟩ directions.

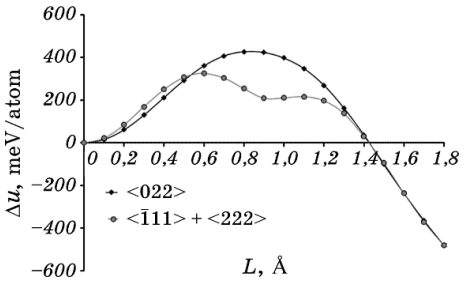

Fig. 3. The specific energy change of an iron nanocluster during the carbon-atom drift in the ⟨011⟩ and $\langle\bar{1}11\rangle$ plus ⟨111⟩ directions.

the nickel atom held one of the positions 1 or 4 (Table 1).

The TIS potential barriers' correlation was more complicated. There were three ratios between the potential barriers of the tetrahedral interstice what a carbon atom may overcome to reach the surface: *a*) $\Delta_1 \approx \Delta_2$, *b*) $\Delta_1 > \Delta_2$ and *c*) $\Delta_1 < \Delta_2$.

Both potential barriers with an accuracy of 5% have the equal height when they corresponded to 11, 12 and 14 positions of nickel atom. In these cases, the heights of potential barriers on the way to the surface through tetrahedral interstice were 13–18% less than in the direction ⟨011⟩. The energy depth of tetrahedral interstices did not exceed 40 meV/atom or 11% between the maximum and the minimum. Although it was unstable in comparison to the case when a carbon atom occupied the octahedral interstice, the position was the most stable of the three cases.

In the second case, the first barrier was higher than the second potential barrier, which included the majority of positions of a nickel atom (*1–9*, *13*) (Fig. 4, light grey arrows). The condition for a carbon atom drifting created to the surface because the nanocluster energy reduced. The energy advantage was from 14 to 20% in comparison to the direction ⟨111⟩. For the carbon atom, the most energy-favourable was

TABLE 1. Nanocluster energy at different positions of a carbon atom and a nickel one at sequential drift of a carbon atom in the direction $\langle\bar{1}11\rangle$ and $\langle 111\rangle$ to the surface: *a*) $\Delta_1 \approx \Delta_2$ (with an accuracy of 5%), *b*) $\Delta_1 > \Delta_2$, *c*) $\Delta_1 < \Delta_2$.

Equivalent Ni atom positions	Ratio	Δ_1	Δ_2	Δ	$\Delta-\Delta_{max1,2}$	$\Delta_{min1,2}/\Delta_{max1,2}$	$(\Delta-\Delta_{max1,2})/\Delta$
		meV/atom				%	
11=14=12	$\Delta_1\approx\Delta_2$	440	425	534 506	94 66	3,4	17,6 13,0
2=5≈3=8=6=7	$\Delta_1>\Delta_2$	368	343	457 458	89 90	6,8	19,5 19,7
4	$\Delta_1>\Delta_2$	368	335	427	59	9,0	13,8
1=9=13	$\Delta_1>\Delta_2$	326	216	427 462	101 136	33,7	13,8 20,3
10	$\Delta_1<\Delta_2$	326	362	506	144	–9,9	28,5

position 1 of a nickel atom.

There was the third case where the height of the second potential barrier of tetrahedral interstice was larger than the first one by 10%. The potential barrier was significantly lower in this case than in $\langle 011\rangle$ direction (by 29%) for the carbon-atom drift to the surface through the TIS, also was the conditions existed for carbon atom returning towards the COIS (Fig. 4, dark grey arrows).

3.2. The Estimation of the Growth Directions of an Iron Nanocluster

The results of the calculations show that the optimal configuration of atoms with minimal energy corresponds to the Ni–C–Fe group of atoms located on the one side of the nanocluster. However, the joining of the additional iron atom from this direction was unlikely according to a calculation. Every one of nanocluster energy with attached an iron atom in every position was estimating (Table 2).

It was established the impurity atoms do not affect in no way the cluster energy in cases when the iron atom joins to cluster in the directions shown in Fig. 5 (see empty balls), *i.e.*, the directions such as $\langle 100\rangle$, $\langle 114\rangle$, *etc.* In these cases, the clusters energy has not changed and the cluster growth was the energy-favourable in the indicated directions (Table 3). In other words, the joining energy was even lower than thermal vibrations energy below of room temperature.

There were determined directions $\langle 311\rangle$, $\langle 131\rangle$, $\langle\bar{1}12\rangle$ and $\langle\bar{1}21\rangle$ (Fig. 6, empty balls), in which the iron-atom addition was possible with energy equal to thermal-vibrations' energy in 300–490 K range.

Such a temperature range corresponds to nanocluster formation during CVD pyrolysis of iron carbonyls [34, 35].

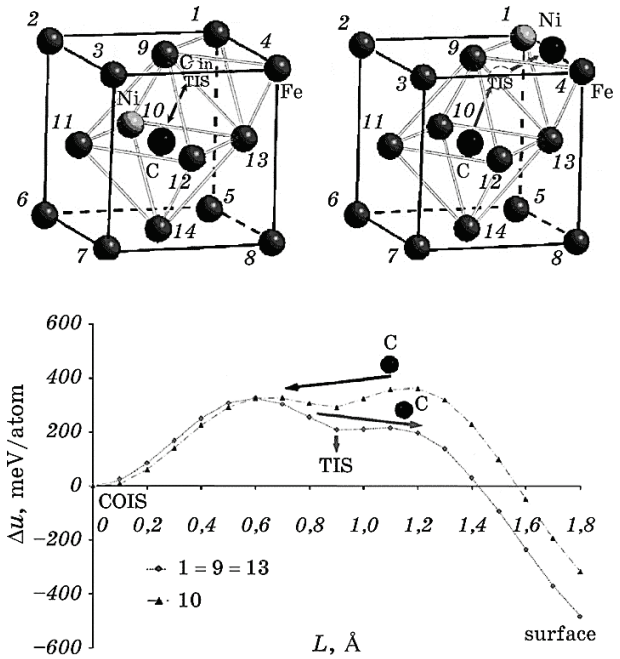

Fig. 4. Scheme of the nickel-atom positions that affect the height of potential barriers the tetrahedral interstice.

TABLE 2. Cluster specific energy at different positions of an iron atom around the f.c.c. Fe–Ni–C frame, where: K is number of atom position in f.c.c. cluster; $\pm i$—X, Y or Z axis; Δu—specific energy (per atom) after addition of one iron atom.

Equivalent positions of Fe atoms around of f.c.c. Fe–Ni–C nanocluster ($K_{\pm i}$)	Δu, meV/atom	Attitude to thermal vibrations
1_{-x}; 1_y; 1_z; 2_{-x}; 2_{-y}; 2_z; 3_x; 3_{-y}; 3_z; 4_x; 4_y; 4_z; 5_{-x}; 5_y; 5_{-z}; 6_{-x}; 6_{-y}; 6_{-z}; 7_x; 7_{-y}; 7_{-z}; 8_x; 8_y; 8_{-z}; 9_z; 10_{-x}; 11_{-y}; 12_x; 13_y; 14_{-z}	–1–0	$\Delta u < \Delta\varepsilon_{kT}$
9_{-x}; 10_y; 10_z; 13_{-x}	60–63	$\Delta u \approx \Delta\varepsilon_{kT}$
9_x; 9_{-y}; 10_{-y}; 10_{-z}; 11_x; 11_{-x}; 11_z; 11_{-z}; 12_{-y}; 12_y; 12_{-z}; 12_z; 13_x; 13_{-z}; 14_x; 14_{-x}; 14_y; 14_{-y}	75–78	$\Delta u > \Delta\varepsilon_{kT}$
9_y; 13_z	239	$\Delta u >> \Delta\varepsilon_{kT}$

The third case corresponds to the energy of the growing cluster, which exceeded the thermal vibrations of atoms at the room temperature (Fig. 7, empty balls). The energy of cluster growth was equal to the thermal vibration energy at 600 K, *i.e.* the temperature range of structural transformation of iron–nickel alloys [36].

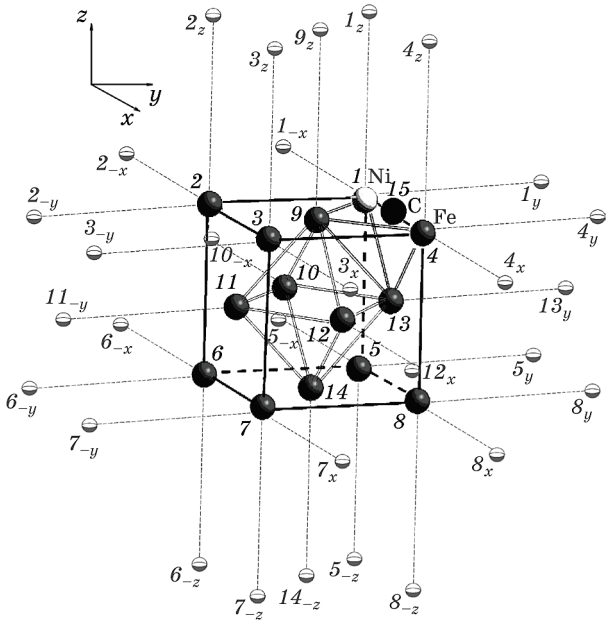

Fig. 5. The probable positions of an iron atom (empty balls), which joins to f.c.c. Fe–Ni–C nanocluster, where is the specific energy (Δu) less than the atom thermal-vibrations' energy ($\Delta\varepsilon_{kT}$), *i.e.* ($\Delta u < \Delta\varepsilon_{kT}$).

TABLE 3. The correspondence of symbols to the directions of joining of an iron atom to f.c.c. nanocluster.

Symbol	1_{-x}	1_y	1_z	2_{-x}	2_{-y}	2_z	3_x	3_{-y}	3_z
Direction	$\langle\bar{1}11\rangle$	$\langle 021\rangle$	$\langle 012\rangle$	$\langle\bar{1}01\rangle$	$\langle 0\bar{1}1\rangle$	$\langle 001\rangle$	$\langle 201\rangle$	$\langle 11\bar{1}\rangle$	$\langle 102\rangle$
Symbol	4_x	4_y	4_z	5_{-x}	5_y	5_{-z}	6_{-x}	6_{-y}	7_x
Direction	$\langle 211\rangle$	$\langle 121\rangle$	$\langle 112\rangle$	$\langle\bar{1}10\rangle$	$\langle 010\rangle$	$\langle 01\bar{1}\rangle$	$\langle 00\bar{1}\rangle$	$\langle 0\bar{1}0\rangle$	$\langle 100\rangle$
Symbol	7_{-y}	7_{-z}	8_x	8_y	8_{-z}	9_z	10_{-x}	11_{-y}	12_x
Direction	$\langle 1\bar{1}0\rangle$	$\langle 10\bar{1}\rangle$	$\langle 210\rangle$	$\langle 120\rangle$	$\langle 11\bar{1}\rangle$	$\langle 114\rangle$	$\langle\bar{1}11\rangle$	$\langle 1\bar{2}1\rangle$	$\langle 411\rangle$
Symbol	13_y	14_{-z}	9_{-x}	10_y	10_z	13_{-x}	9_x	9_{-y}	10_{-y}
Direction	$\langle 141\rangle$	$\langle 11\bar{2}\rangle$	$\langle\bar{1}12\rangle$	$\langle 131\rangle$	$\langle 113\rangle$	$\langle\bar{1}12\rangle$	$\langle 312\rangle$	$\langle 1\bar{1}2\rangle$	$\langle 1\bar{1}1\rangle$
Symbol	10_{-z}	11_x	11_{-x}	11_z	11_{-z}	12_{-y}	12_y	12_{-z}	13_x
Direction	$\langle 11\bar{1}\rangle$	$\langle 301\rangle$	$\langle\bar{1}01\rangle$	$\langle 203\rangle$	$\langle 10\bar{1}\rangle$	$\langle 1\bar{1}1\rangle$	$\langle 131\rangle$	$\langle 11\bar{1}\rangle$	$\langle 321\rangle$
Symbol	13_{-z}	14_x	14_{-x}	14_y	14_{-y}	9_y	13_z		
Direction	$\langle\bar{1}01\rangle$	$\langle 310\rangle$	$\langle\bar{1}10\rangle$	$\langle 130\rangle$	$\langle 1\bar{1}0\rangle$	$\langle 132\rangle$	$\langle 123\rangle$		

Finally, for the last two possible directions of an iron atom joining to

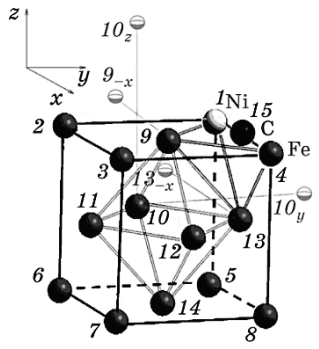

Fig. 6. The probable positions of an iron atom (empty balls), which joins to f.c.c. Fe–Ni–C nanocluster where the specific energy was equal the atom thermal-vibrations' energy ($\Delta u \approx \Delta\varepsilon_{kT}$).

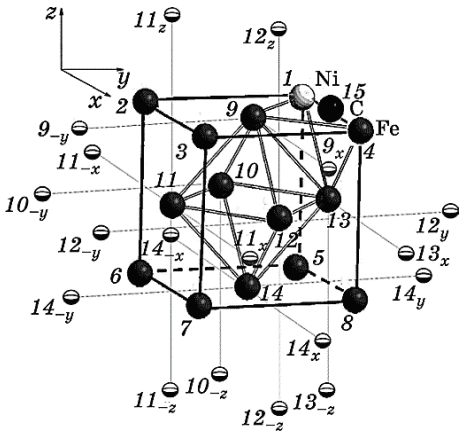

Fig. 7. The probable positions of an iron atom (empty balls), which joins to f.c.c. Fe–Ni–C nanocluster where the specific energy was more than the atom thermal-vibrations' energy ($\Delta u > \Delta\varepsilon_{kT}$).

the nanocluster, namely, ⟨123⟩ and ⟨132⟩ (Fig. 8, empty balls), energy of 239 meV/atom is required, which corresponds to the atom thermal-vibrations' energy at 1850 K. That is in agreement with the temperature range of the Fe–Ni–C phase diagram that corresponds to the iron in the liquid state. Thus, there is an asymmetry of iron nanocluster growth related to the overgrowing of the surface by iron atoms, where the carbon atom is locating (Fig. 9).

4. CONCLUSION

Thus, there are two ways for the carbon atom to drift to the surface of

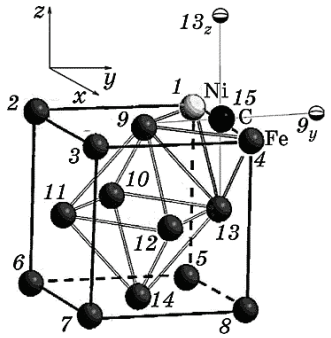

Fig. 8. The probable positions of an iron atom (empty balls), which joins to f.c.c. Fe–Ni–C nanocluster in conditions where the specific energy was much more than the energy of atom thermal vibrations ($\Delta u >> \Delta\varepsilon_{kT}$).

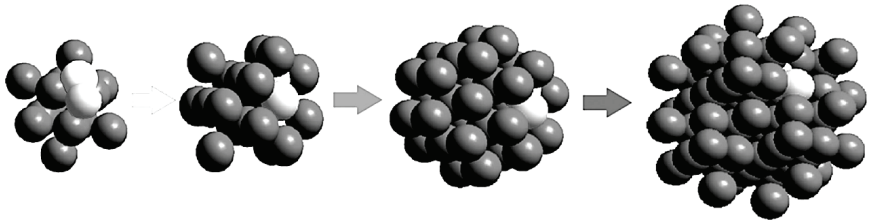

Fig. 9. The growth dynamics of f.c.c. iron nanocluster (the hole near the carbon atom (grey ball) does not overgrow with iron atoms).

the iron f.c.c. nanocluster: the short direction of $\langle 011 \rangle$ with high potential barrier and long direction $\langle 1\bar{1}1 \rangle$ plus $\langle 111 \rangle$, which potential barrier is lower by 13–29%. The carbon atom position is unstable in tetrahedral interstice. So, it can be considering as a transit way of a carbon atom to the surface of the nanocluster.

The nickel atom position affects the height of both potential barriers of tetrahedral interstitial site, and it determines whether is higher. This allows manipulating atoms at the surface of nanocluster.

The impurity atoms affect the joining energy of an iron atom to the f.c.c. Fe–Ni–C nanocluster. When the growth of the iron nanocluster is happening on cubic planes, the carbon atom does not influence on it. However, the carbon atom affects the cluster growth in directions, which form the octahedron within the nanocluster.

The carbon atom on the edge of f.c.c. iron nanocluster is unfavourable for joining of iron atoms from directions $\langle 123 \rangle$ and $\langle 132 \rangle$, which complicates the symmetric growth of the nanoclusters with an interstitial impurity.

These calculations confirmed that the f.c.c. iron–nickel nanocluster is metastable.

REFERENCES

1. B. M. Smirnov, *Cluster Processes in Gases and Plasmas* (Weinheim: Wiley–VCH Verlag GmbH & Co. KGaA: 2010).
2. V. V. Sagaradze, V. E. Danilchenko, Ph. L'Heritier, and V. A. Shabashov, *Mater. Sci. Eng., A*, **337**, Iss. 1–2: 146 (2002).
3. J. A. Alonso, *Structure and Properties of Atomic Nanoclusters* (Singapore: World Scientific: 2005).
4. J. A. Venables, G. D. T. Spiller, and M. Hunbucken, *Rep. Prog. Phys.*, **47**, No. 4: 399 (1984).
5. *Metal Particles and Nanoalloys 3* (Eds. R. L. Johnston and J. Wilcoxon) (Amsterdam: Elsevier Ltd: 2012).
6. F. Baletto and R. Ferrando, *Rev. Mod. Phys.*, **77**, Iss. 1: 371 (2005).
7. L. D. Pachón and G. Rothenberg, *Appl. Organomet. Chem.*, **22**, Iss. 6: 288 (2008).
8. A. K. Singh, *Engineered Nanomaterials: Structure, Properties and Mechanisms of Toxicity* (Amsterdam: Academic Press, Elsevier Inc.: 2016).
9. C. Mottet, G. Rossi, F. Baletto, and R. Ferrando, *Phys. Rev. Lett.*, **95**, Iss. 3: 035501-1 (2005).
10. H. Häkkinen, S. Abbet, A. Sanchez, U. Heiz, and U. Landman, *Angew. Chem. Int. Ed.*, **42**, Iss. 11: 1297 (2003).
11. B. E. Husic, D. Schebarchov, and D. J. Wales, *Nanoscale*, **8**: 18326 (2016).
12. X. G. Ma, Y. F. Liu, N. Liu, J. C. Ren, G. W. Xu, L. Chu, H. Lv, C. Y. Huang, and Y. F. Zhu, *J. Phys. Condens. Matter*, **27**, No. 33: 335301-1 (2015).
13. Z. R. Dai, Sh. Sun, and Z. L. Wang, *Sur. Sci.*, **505**: 325 (2002).
14. J. Diao, K. Gall, and M. L. Dunn, *Nat. Mater*, **2**: 656 (2003).
15. L. D. Pachón and G. Rothenberg, *Appl. Organomet. Chem.*, **22**, Iss. 6: 288 (2008).
16. S. Khanal, A. Spitale, N. Bhattarai, D. Bahena, J. J. Velazquez-Salazar, S. Mejía-Rosales, M. M. Mariscal, and M. José-Yacaman, *Beilstein J. Nanotechnol.*, **5**: 1371 (2014).
17. M. C. Patterson, B. F. Habenicht, R. L. Kurtz, L. Liu, Y. Xu, and Ph. T. Sprunger, *Phys. Rev. B*, **89**, Iss. 20: 205423-1 (2014).
18. L. Liu, J. Yuan, L. Cheng, and J. Yang, *Nanoscale*, **9**, Iss. 2: 856 (2017).
19. M. G. Taylor and G. Mpourmpakis, *Nat. Commun.*, **8**: 15988-1 (2017).
20. F. Kh. Mirzoev and L. A. Shelepin, *Tech. Phys. Lett.*, **28**, Iss. 1: 6 (2002).
21. L. J. Swartzendruber, V. P. Itkin, and C. B. Alcock, *J. Phase Equilib. Diffus.*, **12**, Iss. 3: 288 (1991).
22. *Nanostructured Materials: Sciences & Technology* (Eds. G.-M. Chow and N. I. Noskova) (USA: Kluwer Academic Publishers: 1998).
23. V. G. Gavriljuk, *J. Phys. IV France*, **112**: 51 (2003).
24. P. Yu. Volosevitch, V. V. Girzhon, and V. E. Danil'chenko, *Scripta Mater.*, **37**, Iss. 7: 977 (1997).
25. *Iron Systems. Part 1* (Eds. G. Effenberg and S. Ilyenko) (Berlin–Heidelberg: Springer: 2008).
26. E. G. Lewars, *Computational Chemistry: Introduction to the Theory and Applications of Molecular and Quantum Mechanics* (Berlin: Springer Science Business Media BV: 2011).
27. K. I. Ramachandran, G. Deepa, and K. Namboori, *Computational Chemistry*

and Molecular Modelling. Principles and Applications (Heidelberg: Springer-Verlag: 2008).
28. Q. Yang and A. C. To, *Comput. Methods Appl. Mech. Eng.*, **283**: 384 (2015).
29. H. M. Ledbetter and R. P. Reed, *J. Phys. Chem. Ref. Data*, **2**, Iss. 3: 531 (1973).
30. T. Halicioğlu and G. M. Pound, *Phys. Status Solidi A*, **30**, Iss. 2: 619 (1975).
31. M. Riech, *Nano-Engineering in Science and Technology. An Introduction to the World Nano-Design* (Singapore: World Scientific Publishing Co Pte Ltd: 2003).
32. J. P. Stark, *Solid State Diffusion* (New York: John Wiley and Sons: 1976).
33. A. V. Nedolya and N. V. Bondarenko, *Selected Proceedings of the 4th Int. Research and Practice Conf. 'Nanotechnology and Nanomaterials NANO-2016' (Aug. 24–27, 2016, Lviv, Ukraine). Springer Proceedings in Physics* (Cham, Switzerland: Springer: 2017), vol. **195**, p. 395.
34. K. S. Sree Harsha, *Principles of Physical Vapor Deposition of Thin Films* (Oxford: Elsevier Ltd: 2006).
35. P. Zhang, E. Mohimi, T. K. Talukdar, and J. R. Abelson, *J. Vac. Sci. Technol. A*, **34**, Iss. 5, Art. No. 051518 (2016).
36. I. G. Kabanova, V. V. Sagaradze, N. V. Kataeva, and V. E. Danil'chenko, *Phys. Metals. Metallogr.*, **112**: 381 (2011).